Check for updates

Lithium–Sulfur Batteries

Zitierweise: *Angew. Chem. Int. Ed.* **2020**, *59*, 22150–22155
Internationale Ausgabe: doi.org/10.1002/anie.202008911
Deutsche Ausgabe: doi.org/10.1002/ange.202008911

Direct Intermediate Regulation Enabled by Sulfur Containers in Working Lithium–Sulfur Batteries

Jin Xie, Yun-Wei Song, Bo-Quan Li, Hong-Jie Peng,* Jia-Qi Huang und Qiang Zhang**

Abstract: *Polysulfide intermediates (PSs), the liquid-phase species of active materials in lithium–sulfur (Li-S) batteries, connect the electrochemical reactions between insulative solid sulfur and lithium sulfide and are key to full exertion of the high-energy-density Li-S system. Herein, the concept of sulfur container additives is proposed for the direct modification on the PSs species. By reversible storage and release of the sulfur species, the container molecule converts small PSs into large organosulfur species. The prototype di(tri)sulfide-polyethylene glycol sulfur container is highly efficient in the reversible PS transformation to multiply affect electrochemical behaviors of sulfur cathodes in terms of liquid-species clustering, reaction kinetics, and solid deposition. The stability and capacity of Li-S cells was thereby enhanced. The sulfur container is a strategy to directly modify PSs, enlightening the precise regulation on Li-S batteries and multi-phase electrochemical systems.*

Introduction

The sustainable growth of renewable energy sources, electric vehicles, and advanced electronic devices demands energy storage systems with higher energy density and lower cost.[1] As one of the most promising energy storage systems, lithium-sulfur (Li-S) battery has attracted broad interests for the high theoretical energy density of 2600 Wh kg^{-1} and low cost of abundant source materials.[2] Unfortunately, the low electrical conductivity of solid sulfur species (sulfur and lithium sulfide) renders sulfur-based materials poor electrochemical reactivity regarding the solid-phase-involved reactions. Soluble polysulfide intermediates (PSs) connect the insulate sulfur and sulfide via the solid–liquid-solid multiphase processes involving repeated dissolution and deposition of solid sulfur and Li_2S.[3] PSs themselves serve as intrinsic redox mediators to activate the solid phases and transport electrons at the conductive interfaces.[4] Therefore, the performances of sulfur cathode are largely determined by the redox behaviors of PSs in the liquid electrolyte.

The amount and state of PSs in Li-S cells are mainly determined by the depth of discharge (DOD). The high-order PSs ($Li_2S_{6\text{-}8}$) are generated from bulk sulfur and their amounts increase with increasing DOD and then reduced to low-order Li_2S_4 at a moderate DOD of around 25%.[5] The concentration of PSs in electrolyte comes to the maximum at the beginning of the low-voltage discharge plateau, which is usually attributed to the deposition of $Li_2S_{(2)}$ from Li_2S_4.[4] However, the above native evolution of PSs regarding the concentration and redox states cannot fully meet the demands for stably and efficiently manipulating the multi-phase transformation of sulfur and sulfide.[6] First, the limited solubility and activity of PSs such as Li_2S_4 retard the kinetics of solid precipitation. Second, the relatively low concentration of PSs affords limited ability in activating the solid bulks, thereby causing high overpotential with reduced specific energy.[7] Moreover, the mobility of PSs is regarded as a double-edged sword. On one hand, it enables PSs as internal redox mediators; on the other hand, it induces fluctuation of the PS distribution within the cathode chamber and also shuttle effects in a working battery.[8] To fully exert the merits of PSs in mediating the reaction kinetics while prevent the side effects, the regulation of concentration, state, and distribution of PSs is of great significance for high-performance Li-S batteries.

To regulate the behavior of PS intermediates in a Li-S battery, various extrinsic regulation strategies based on physical confinement or chemical adsorption/catalysis are proposed.[9] Physical confinement restricts the dispersion of PSs at the anode by selective building blocks such as Nafion,[10] graphene oxide,[11] and MOF,[12] which can efficiently suppresses the shuttle of PS intermediates.[13] However, the activity of PSs cannot be instantly mediated, where kinetic challenges remain in a working battery. Chemical adsorptive/catalytic materials such as metal carbides,[14] nitrides,[15] chalcogenides,[16] single atom sites,[17] and their carbon composites[18] effectively work in mediating the PS activity on electrochemical active interfaces. However, such modification on the electrode–electrolyte interfaces is unable to completely address the dissolved PSs away from the cathode chamber.[19] To this end, homogeneous regulation in liquid phase, such as the use of redox mediator (RM), is reported to mediate the dissolved PSs by providing alternative chemical routes for the sulfur redox reactions.[7a,20] Nevertheless, RMs cannot intrinsically change the evolution and the chemical state of PSs, leaving problems such as anode corruption and shuttle ef-

[*] J. Xie, Y.-W. Song, Prof. Q. Zhang
Beijing Key Laboratory of Green Chemical Reaction Engineering and Technology, Department of Chemical Engineering
Tsinghua University, Beijing 100084 (P. R. China)
E-Mail: zhang-qiang@mails.tsinghua.edu.cn
Dr. B.-Q. Li, Prof. J.-Q. Huang
School of Materials Science & Engineering
Beijing Institute of Technology
Advanced Research Institute of Multidisciplinary Science
Beijing Institute of Technology, Beijing 100084 (P. R. China)
E-Mail: libq@bit.edu.cn
Dr. H.-J. Peng
Department of Chemical Engineering, Stanford University
Stanford, CA 94305 (USA)
E-Mail: hjpeng@stanford.edu
Supporting information and the ORCID identification number(s) for the author(s) of this article can be found under: https://doi.org/10.1002/anie.202008911.

fect.[21] Considering the defects of the extrinsic regulation methods, direct chemical modification of the dissolved intermediates in liquid phase is highly demanded to offset the problems caused by sub-optimal concentration, distribution, and chemical activity of PSs in working batteries.

Herein, a polymer organosulfur additive of di(tri)sulfide polyethylene glycol (PES_n) is proposed as the prototype of the concept of sulfur containers, which is expected to directly regulate the PS intermediates in a working sulfur electrode. The sulfur container in electrolyte can storage and release sulfur atoms through the reversible reactions with the soluble sulfur species. Consequently, the soluble PS intermediates in routine Li-S batteries were substituted by the organic PS containers, resulting in the overall regulation of the liquid sulfur species (Figure 1). Polyether chains are grafted with (di/tri)sulfide bonds on each side to form the chemical structure of a sulfur container. The (di/tri)sulfide bonds render robust sulfur storage and release by reversibly lengthening and shortening the sulfur chains, which is in accordance with organosulfur electrochemistry.[22] Besides, the polyether segments were introduced to mediate the (di/tri)sulfide groups. The polyether segments with an ether-like structure not only control the dissolution/migration behavior, but provide special co-solvent environment of the (di/tri)sulfide groups as well. The modification of the intermediates by PES_n displayed multiple advantages on the electrochemical behaviors of Li-S batteries, including regulated chain length distribution, enhanced electrochemical kinetics, and novel liquid-solid deposition morphology of the PS species. Consequently, Li-S cells with PES_n containers were enhanced in both capacity and stability.

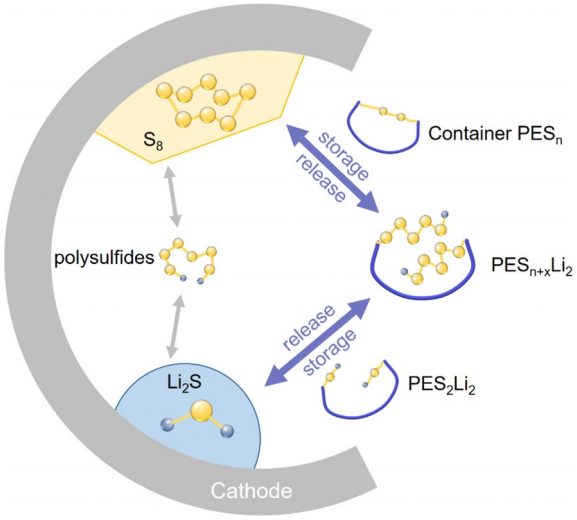

Figure 1. The working mechanism of sulfur container PES_n in working Li-S batteries.

Results and Discussion

The sulfur container PES_n derived from dithio-polyether (HS-PE-SH) was synthesized by thermally induced substitute reactions with sulfur powder. Each polyether segment is connected by (di/tri)sulfide functional groups on both sides. The (di/poly)sulfides groups ($-S_{(n)}-$) serve as the sulfur storage/release active sites to accommodate sulfur atoms from sulfur and PSs and feed sulfur atoms to the lithium sulfide. The large polyether chain was designed to stabilize the sulfur sites (Supporting Information, Figure S1). Typically, the average molecular weight of polyether segment was 1×10^3 according to hydrogen nuclear magnetic resonance (^{1}H-NMR) spectrum (Supporting Information, Figure S2). Such a polyether chain loaded with (di/poly)sulfide bonds is large enough to determine the main physical properties of PES_n such as the solubility and mobility in electrolyte and to mediate the chemical environment of the sulfur containing groups.

The sulfur container PES_n displayed high reactivity in sulfur storage and release processes. As revealed by the visible chemical reactions between PES_n and Li_2S_8 (Supporting Information, Figure S3), the mixture solution instantly turned light orange, indicating the production of R-S_xLi via the cleavage and rearrangement of the sulfur chains in PES_n and Li_2S_8. The fast color evolution revealed high chemical activity of PES_n to absorb PSs. Bulk Li_2S can also be stored in PES_n to form LiS-PE-S_nLi, as the white Li_2S suspension instantly turned yellow after mixing with PES_n. The ability to chemically react with solid bulk Li_2S enabled PES_n to activate the dead sulfur species that were detached away from the electrochemical conductive surface. UV/Vis spectra reveal the change of sulfur chains in the sulfur storage reactions between PES_n and LiPSs (Figure 2a). The disulfide bond of PES_n with a signal of 380 nm vanished, while a new signal of 480 nm (S_6^{2-}) was found after the reactions with Li_2S_8, which is assigned to the evolution of disulfide bonds to R-S_nLi. The rearrangement of the sulfur chains was further investigated by the relative intensity of different polysulfide ion fragments in positive matrix-assisted laser desorption/ionization time of flight mass spectrometry (MALDI-TOF-POS-MS) measurements (Figure 2b). Free Li_2S_8 slurry displayed dominant S_5^+ and S_3^+ signals, indicating the tendency of PS decomposition from S_8 to S_5+S_3 during the online measurement. There were still 3% S_8^+ and 2% $S_4^+(S_8^{2+})$ remained, which corresponded to preserved S_8 chain and minor degradation pathway for S_8 to two S_4. The relative intensity of S_5^+ was enhanced from 87 to 98% with PES_n, while the S_3^+, S_8^+, and $S_4^+(S_8^{2+})$ signal diminished. The reduced S_8^+ proved that PES_n induced the cleavage of S_8 chains in Li_2S_8 solution, while the enhanced S_5^+ and vanished S_3^+ indicate that the sulfur fragments S_3 and S_5 are rearranged with (di/poly)sulfide bonds to form R-S_xLi ($x>4$).[23] The sulfur rearrange mechanism endowed PES_n with rapid sulfur modification ability by reversibly lengthening/shortening the sulfur chains connected to the polyether chains.[24] The efficient regulation of PS intermediates is supposed to mediate the entire behavior of the sulfur cathode such as PS composition, kinetics of liquid phase reactions, deposition morphology, and therefore the cyclic performance.

To fully identify the actual capacity of PES_n for sulfur storage/release under electrochemical environments, quantitative experiment was designed as follows. There are three typical state of the container in battery: the fully charged state PES_n, the largest storage state $PES_{n+x}Li_2$, and the fully di-

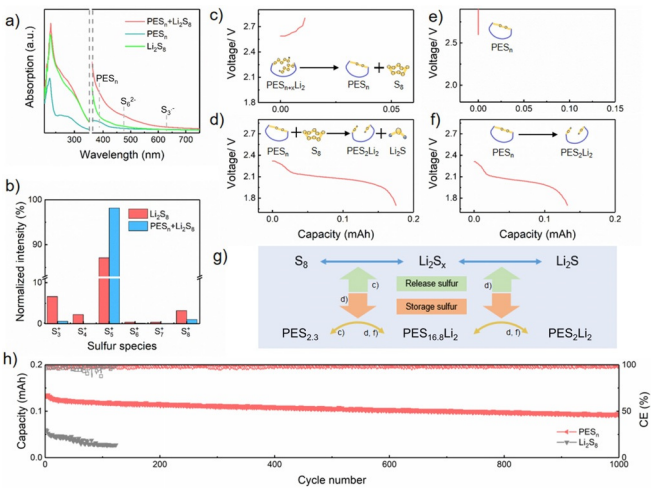

Figure 2. Chemical interactions and electrochemical properties of PES_n. a) UV/Vis spectrum of $Li_2S_8+PES_n$, in comparison with PES_n and Li_2S_8 solution in DOL/DME. b) MALDI-TOF-POS-MS signal of different sulfur fragments in Li_2S_8 solution with or without PES_n. c),d) The first charge and discharge profile of sulfur storage state container PE-$(S_mLi)_2$. e),f) The first charge and discharge profile of oxidized state container PES_n. g) The sulfur release and storage diagram of sulfur container PES_n, the conversion occurred in (c)–(f) were marked near the relative arrows. h) The cycling stability of the sulfur container $PES_{2.3}$ in comparison with Li_2S_8.

scharged state PES_2Li_2. Firstly, the largest storage state $PES_{n+x}Li_2$ was prepared by the reactions between fully discharged state PES_2Li_2 and S_8. Then $PES_{n+x}Li_2$ was fully charged to 2.8 V, then discharged to 1.7 V, of which the charge and discharge capacity are Q_1 and Q_2, respectively. Besides, the initial charged state PES_n was charged and discharged with capacities of Q_3 and Q_4 (Figure 2c–f). The charging and discharging reactions are concluded as:

$$PES_{n+x}Li_2 - 2e^- - 2Li^+ \xrightarrow{\text{charging}} PES_n + (x/8)S_8 \quad (Q1)$$

$$PES_n + (x/8)S_8 + (2x+2n-2)(Li^+ + e^-) \xrightarrow{\text{discharging}} PES_2Li_2 + (x+n-2)Li_2S \quad (Q2)$$

$$PES_n \xrightarrow{\text{charging}} PES_n \quad (Q3)$$

$$PES_n + (2n-2)e^- + (2n-2)Li^+ \xrightarrow{\text{discharging}} PES_2Li_2 + (n-2)Li_2S \quad (Q4)$$

The values of x and n were calculated by the capacities Q_1, Q_2, Q_3, and Q_4 according to the reaction model above:

$$\begin{cases} x = \frac{Q_2 - Q_4}{Q_1} \\ n = 1 + \frac{Q_4}{Q_1} \end{cases}$$

$$Q_3 = 0$$

The measured capacities of Q_1, Q_2, and Q_4 of 0.102, 1.614, and 0.134 mAh determine the n and x value of 2.3 and 14.5, respectively. Consequently, the (di/tri)sulfide bond of PES_n displays an average sulfur atomic number of 2.3, which hints a composition of 30% trisulfide and 70% disulfide. The maximum sulfur storage capacity is 14.5 sulfur atoms per (di/tri)sulfide bonds. The stored-state container $PES_{16.8}Li_2$ consist of two R-$S_{8.4}$Li, revealing that the dominant sulfur chain in electrolyte herein is dominantly R-S_8-Li chain (Figure 2g). After full discharge, the stored-state $PES_{16.8}Li_2$ can release 14.8 lithium sulfide and results in PES_2Li_2. The quantitative sulfur storage/release ability of $PES_{2.3}$ directs the precise PS chemical modification in lithium sulfur batteries.

The design of organic residue mediates the chemical situation of the sulfur sites in PES_n, which potentially mediates the electrochemical behavior of sulfur. To find out the effect in electrochemistry, $PES_{2.3}$ and ordinary LiPSs was introduced as active materials in catholyte for cycling test, respectively. $PES_{2.3}$ of 0.002 mmol in molar amount as active materials displayed high cycling stability at 1 mA, with a capacity retention of 73.9% after 500 cycles and 66.2% after 1000 cycles (Figure 2h). In comparison, Li_2S_8 battery with 0.002 mmol sulfur atoms rapidly faded by 60.7% in capacity after 120 cycles from 0.061 to 0.024 mAh, with a retention of 39.3%. The superior electrochemical stability of $PES_{2.3}$ is related to two factors modified by polyether residues. One is the high solubility of discharged product PES_2Li_2, which prevents the random precipitation of solid Li_2S discharge products in electrochemical inactive regions. The other one is the large polyether groups connected to sulfur sites to protect the sulfur species from fast diffusion and accompanying reaction in the anode side. With PES_n, the chemical corrosion of lithium metal by Li_2S_8 electrolyte was controlled (Supporting Information, Figure S4). As a result, the high Coulombic efficiency (CE) around 99% in 1000 cycles of $PES_{2.3}$ was achieved. The large difference in cyclic performances between polymeric container and inorganic LiPSs indicates the significance of PS modification in working batteries.

Considering the high chemical reactivity of PS modification, using sulfur container PES_n should be an effective method to change the chemical state and distribution at different DODs of PS molecules in Li-S cells. To evaluate the modification effect in Li-S batteries, in situ Raman spectrum of electrolyte was applied (Figure 3a,b) to trace the PS signal change in sulfur/carbon cathode during the voltammetric discharging process from 2.7 to 1.8 V at 0.1 mV s^{-1}. Especially, sulfur chain signal of different polysulfide species was focused to understand the sulfur speciation evolution. With $PES_{2.3}$, the intensity of long-chain PSs was observed earlier at 2.4 V, revealing the accelerated reduction of sulfur solid to polysulfides. The short PS vibration such as S_4^{2-}/R-S_4^- at 500–510 cm^{-1} and 460–470 cm^{-1} was strengthened during the discharging from 2.4 to 2.0 V, validating an enhanced PS conversion.[25] The enhancement in PS signals at higher potentials indicates the participation of PES_n in the storage/release of sulfur species, indicating effective PS regulation by the sulfur container. At a lower voltage with below 2.0 V, the signal of short polysulfides and disulfides at 195–200 cm^{-1} such as Li_2S_2 and R-S_2Li was observed in the PES_n contained electrolyte, proving an enhanced reductive reaction of the sulfur intermediates. In a word, the sulfur containing agent $PES_{2.3}$ efficiently mediates the sulfur dissolution and liquid phase PS evolution through the storage/release pathway. Moreover, Raman spectrum excited by laser of 633 nm in wavelength

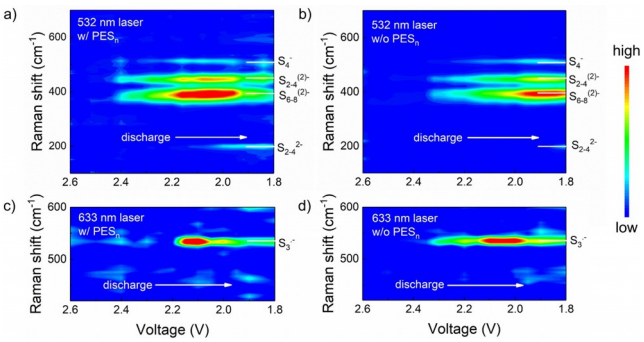

Figure 3. In situ Raman spectrum during the discharging process of Li-S batteries a) with and b) without PES_n at an excitation wavelength of 532 nm; c) with and d) without PES_n at an excitation wavelength of 633 nm.

traced the resonance signal of radical $S_3^{\bullet-}$ symmetric vibration around 536 cm^{-1}. The radical $S_3^{\bullet-}$ peak was found sharpened and raised earlier in battery with PES_n (Figure 3c,d).[26] The $S_3^{\bullet-}$ intensity change is attributed to the influence of polyether chains, considering that radical $S_3^{\bullet-}$ can be stabilized in high donor-number solution.[27] Radical $S_3^{\bullet-}$ is regarded as one of the most active species in the chemical reactions between PSs, therefore also contributes to the chemical regulation by sulfur containers in kinetic acceleration of sulfur conversion in liquids.[28]

The regulation caused by $PES_{2.3}$ obviously changed the composition and activity of liquid PS intermediates, so as to regulate the solid–liquid deposition. The deposition morphology was further observed by optical microscopy, revealing the special sulfur release-deposition reaction from mediated sulfur species PES_xLi_2 to Li_2S and Li_2S_2 (Supporting Information, Figure S5). Generally, the discharged cathode mediated by $PES_{2.3}$ displayed uniform transparent dark yellow drop-like deposition via optical lens, in comparison with the ordinary translucent lemon bulks. Scanning electron microscopy (SEM) further showed the details of the special deposition induced by $PES_{2.3}$. Spindle-shape $Li_2S_{(2)}$ of 5 to 50 µm was found on carbon fiber hosts, which is smooth and symmetric (Figure 4a,b). However, the deposition from Li_2S_8 is rough and irregular thin coatings.[29] The larger and uniform spindle deposition of Li_2S indicates a larger deposition capacity with $PES_{2.3}$ on the same electrochemical surface area, which matches the stronger Raman signal of $Li_2S_{(2)}$. The special morphology with shape uniformity and tight connection with carbon substrate is preferred for sulfur cathode with high reversibility and capacity. Corresponding energy dispersive spectrum (EDS) mapping displayed the sulfur release of PES_xLi_2 in $Li_2S_{(2)}$ electrodeposition (Figure 4c,e). The sulfur signal was mainly found in the deposition solids, while the carbon signal was detected in exposed carbon fibers. However, the oxygen signal was observed both on carbon fibers and the surface of sulfur deposition, proving the distribution of the polyether-based sulfur container PES_xLi_2 and PES_2Li_2 at the electrolyte/$Li_2S_{(2)}$ interfaces. Linear sweep EDS spectrum across the carbon fiber further reveals the coaxial oxygen rich layer/sulfur rich layer on carbon cable, indicating that an organosulfur layer was formed on the solid–

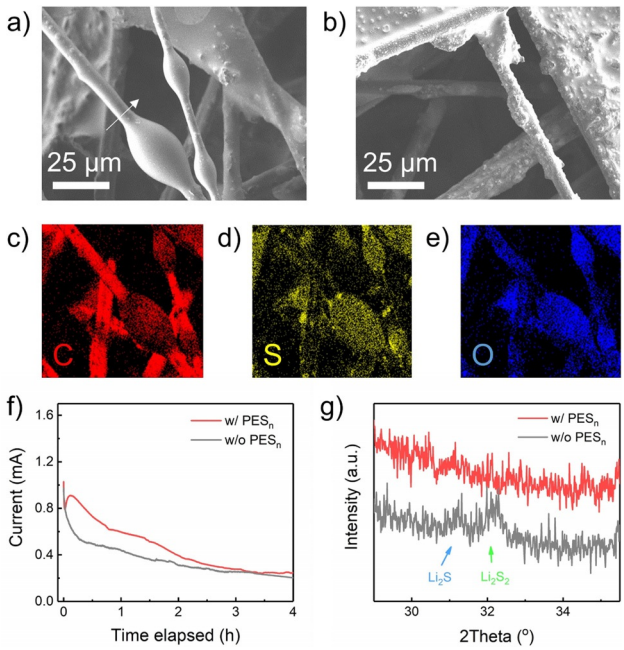

Figure 4. The morphology of lithium sulfide deposition. a),b) SEM images of the Li_2S deposition on carbon paper surface after discharging with and without PES_n. c)–e) Corresponding EDS mapping of carbon, sulfur, and oxygen element in the Li_2S deposition with PES_n addition. f) Nucleation test of polysulfides–carbon paper cathode at 2.0 V, and corresponding in situ XRD pattern after a nucleation time of 4 h with and without PES_n.

liquid interface (Supporting Information, Figure S6). The existence of PES_xLi_2 interface indicates that regulated PSs are preferred in participating in the interfacial charge transfer and sulfur migration, inducing the special morphology. There are multiple mechanisms for the stronger interfacial activity of PSs regulated by sulfur containers, such as the higher donor number of polyether surrounding the sulfur chain than ordinary solvents and the interfacial affinity of polymer sulfur containers to regulate the distribution of sulfur. The special morphology indicates great potential of PS regulation by sulfur containers in enhancing liquid-solid reactions with high reversibility and capacity. Revealed by nucleation test at 2.0 V (Figure 4f), strengthened current peaks after a potentiostatic time of 450 s and a larger capacity of Li_2S deposition could be found with PES_n, corresponding to a preferred liquid–solid deposition efficiency influenced by PS regulation. In situ X-ray diffraction patterns of the carbon paper cathode after the nucleation test further revealed the different crystalline behaviors of the solids deposited from PSs with and without regulation (Figure 4g). The spindle-shape $Li_2S_{(2)}$ are mainly amorphous since no obvious diffraction signal of typical Li_2S (200) or reported Li_2S_2 was observed with PES_n. The amorphization of solid species affected by PES_n is proposed to enhance the reversibility of liquid–solid conversions as large Li_2S crystal is regarded difficult to be activated.

The influence of PS regulation by sulfur container in kinetics was then detected in symmetric cells. Cyclic voltammetry (CV) measurement showed an enlarged polarity current at 0.4 V from 12 to 16 mA with $PES_{2.3}$, proving the kinetic enhancement by 1/3 (Figure 5a). Additionally, the interfacial

impedance of 82 ohm in battery with containers is much lower than the control Li_2S_6 cell without containers (Figure 5b).[16b,30] These results confirmed the kinetic promotion as well as the reduced impedance spectra. The kinetic enhancement confirmed the higher electrochemical activity of the regulated PSs by the sulfur containers. With preferred sulfur concentration regulation and sulfur kinetics endowed by the sulfur containers, the capacity and reversibility of sulfur cathode are enhanced.

The sulfur container $PES_{2.3}$ was applied in the electrolyte of Li-S battery to probe the effect of direct sulfur regulation. Considering $PES_{2.3}$ with a sulfur storage capacity of 14.8 sulfur atoms, 20 µL cathodic electrolyte containing 10 wt% $PES_{2.3}$ (0.15 mg sulfur) can chemically modify PSs equivalent to 1.0 mg sulfur from the cathode. Since that $PES_{2.3}$ only substituted part of the solvent weight in electrolyte, the overall amount of electrolyte does not increase. Carbon nanotube/sulfur composite cathode with a sulfur loading of 1.2 mg cm^{-2} was applied for measurement. With the containing agent $PES_{2.3}$, the initial capacity was efficiently enhanced from 833 to 1009 mAh g^{-1} at 0.5 C, calculated based on the sulfur amount in cathode (Figure 5c). After 100 cycles, a higher capacity of 748 mAh g^{-1} is remained in the presence of $PES_{2.3}$ than the control group of only 510 mAh g^{-1}. Considering the additional capacity contributed by the electrochemical activity of $PES_{2.3}$ of 0.139 mAh (87 mAh g^{-1}), the actual enhancement in discharging capacity endowed by the sulfur storage/release effect is 89 mAh g^{-1} at the first cycle and 151 mAh g^{-1} after 100 cycles (Figure 5c; Supporting Information, Figure S7). Consequently, both enhancements in capacity and cycling stability were observed in batteries with the sulfur container. Discharging and charging profile further revealed the details of performance enhancement: both the higher and lower discharging stages are lengthened by $PES_{2.3}$. The capacity promotion at both stages indicates that both the solid–liquid reaction from sulfur to dissolved PSs and the liquid–solid deposition are activated by $PES_{2.3}$. Moreover, the voltage of the initial discharging stage was raised up by 20 mV, which is attributed to the special sulfur transforming route from S_8 to stored state $PES_{16.8}Li_2$ different from conventional Li_2S_8. However, the lower stage exhibited a slight lower but stable voltage profile, which was related to the different deposition kinetics corresponding to the sulfur release from PES_xLi_2 to Li_2S (Figure 5d). To understand the compatibility of PS regulation by sulfur container in practical Li-S battery, $PES_{2.3}$ was evaluated with cathodes of a sulfur loading of 3.6 mg cm^{-2} (Supporting Information, Figure S8). The high loading Li-S battery with $PES_{2.3}$ displayed stable cycles with a maximum capacity of 970 mAh g^{-1} at 0.1 C, facilitating the possibility for further practical applications.

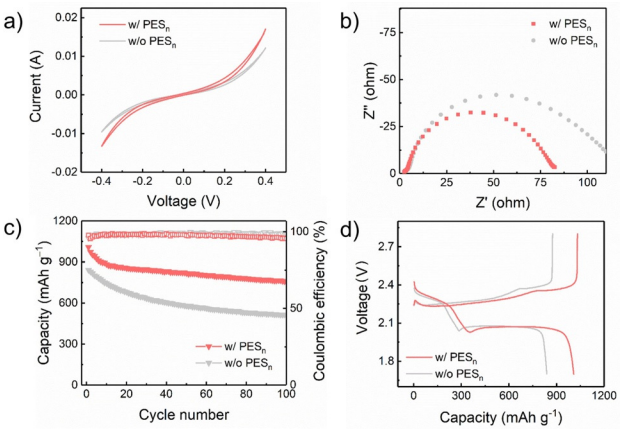

Figure 5. Kinetic characterization and cycling performances of Li-S batteries with and without PES_n. a) CV profile at the scanning rate of 0.1 V s^{-1} and b) EIS spectrum of Li_2S_6 symmetric cell. c) Cycling performances of the Li-S battery with and without PES_n. d) Corresponding charge and discharge profiles.

Conclusion

The direct regulation of liquid intermediates in Li-S battery was proposed and investigated by applying a polymeric sulfur container $PES_{2.3}$. The sulfur container $PES_{2.3}$ displayed a rapid regulation of PSs by quantitatively lengthening and shortening the sulfur chain sites. Each $PES_{2.3}$ displayed a maximum sulfur storage/release capacity of 14.5/14.8 sulfur atoms during the discharging process. The different chemical properties of the polyether modified PES_xLi from routine Li_2S_x induced the multiple changes of sulfur cathode behaviors. With $PES_{2.3}$, the concentration and distribution of sulfur chains were mediated, in which low order (poly)sulfides were observed earlier. Besides, the liquid-solid behavior with $PES_{2.3}$ facilitates a unique and preferred deposition phenomenon. Moreover, the kinetics of PSs was enhanced under the modification of $PES_{2.3}$. The multiple influences on sulfur electrode resulted in an enhancement in the capacity and stability of Li-S battery by 151 mAh g^{-1} after 100 cycles. The direct PS regulation by PES_n with corresponding chemical understanding provides an effective way to the mediation of sulfur chemistry in Li-S battery and directs the precise regulation of intermediates in multi-electron redox reactions in a working battery.

Acknowledgements

This work was supported by the National Natural Science Foundation of China (21776019, 21825501, and U1801257), National Key Research and Development Program (2016YFA0202500), and the Tsinghua University Initiative Scientific Research Program. We thank Meng Zhao, Chang-Xin Zhao, Xue-Qiang Zhang, Dr. Hong Yuan, Dr. Gao-Long Zhu for helpful discussion.

Conflict of interest

The authors declare no conflict of interest.

Stichwörter: lithium polysulfide · lithium-sulfur batteries · organosulfur · sulfur chemistry · sulfur container

[1] a) R. Fang, S. Zhao, Z. Sun, W. Wang, H.-M. Cheng, F. Li, *Adv. Mater.* **2017**, *29*, 1606823; b) Z. Li, H. B. Wu, X. W. Lou, *Energy Environ. Sci.* **2016**, *9*, 3061–3070; c) Q. Pang, X. Liang, C. Y. Kwok, L. F. Nazar, *Nat. Energy* **2016**, *1*, 16132; d) H.-J. Peng, J.-Q. Huang, Q. Zhang, *Chem. Soc. Rev.* **2017**, *46*, 5237–5288.

[2] a) A. Manthiram, Y. Z. Fu, Y. S. Su, *Acc. Chem. Res.* **2013**, *46*, 1125–1134; b) H. J. Peng, J. Q. Huang, X. B. Cheng, Q. Zhang, *Adv. Energy Mater.* **2017**, *7*, 1700260; c) Y. Liang, C. Z. Zhao, H. Yuan, Y. Chen, W. Zhang, J. Q. Huang, D. Yu, Y. Liu, M. M. Titirici, Y. L. Chueh, H. Yu, Q. Zhang, *InfoMat* **2019**, *1*, 6–32; d) X.-B. Cheng, C.-Z. Zhao, Y.-X. Yao, H. Liu, Q. Zhang, *Chem* **2019**, *5*, 74–96.

[3] a) Z. Li, L. X. Yuan, Z. Q. Yi, Y. M. Sun, Y. Liu, Y. Jiang, Y. Shen, Y. Xin, Z. L. Zhang, Y. H. Huang, *Adv. Energy Mater.* **2014**, *4*, 1301473; b) S. Waluś, C. Barchasz, J. F. Colin, J. F. Martin, E. Elkaïm, J. C. Leprêtre, F. Alloin, *Chem. Commun.* **2013**, *49*, 7899–7901.

[4] F. Y. Fan, W. C. Carter, Y. M. Chiang, *Adv. Mater.* **2015**, *27*, 5203–5209.

[5] a) A. F. Hofmann, D. N. Fronczek, W. G. Bessler, *J. Power Sources* **2014**, *259*, 300–310; b) G. R. Li, S. Wang, Y. N. Zhang, M. Li, Z. W. Chen, J. Lu, *Adv. Mater.* **2018**, *30*, 1705590.

[6] a) R. Xu, I. Belharouak, J. C. M. Li, X. F. Zhang, I. Bloom, J. Bareno, *Adv. Energy Mater.* **2013**, *3*, 833–838; b) H. Yamin, A. Gorenshtein, J. Penciner, Y. Sternberg, E. Peled, *J. Electrochem. Soc.* **1988**, *135*, 1045–1048; c) H. Yuan, H. J. Peng, B. Q. Li, J. Xie, L. Kong, M. Zhao, X. Chen, J. Q. Huang, Q. Zhang, *Adv. Energy Mater.* **2019**, *9*, 1802768.

[7] a) L. C. H. Gerber, P. D. Frischmann, F. Y. Fan, S. E. Doris, X. Qu, A. M. Scheuermann, K. Persson, Y. M. Chiang, B. A. Helms, *Nano Lett.* **2016**, *16*, 549–554; b) X. Liang, C. Hart, Q. Pang, A. Garsuch, T. Weiss, L. F. Nazar, *Nat. Commun.* **2015**, *6*, 5682.

[8] a) N. Deng, W. Kang, Y. Liu, J. Ju, D. Wu, L. Li, B. S. Hassan, B. Cheng, *J. Power Sources* **2016**, *331*, 132–155; b) J. Liang, Z.-H. Sun, F. Li, H.-M. Cheng, *Energy Storage Mater.* **2016**, *2*, 76–106; c) H. Wang, W. Zhang, J. Xu, Z. Guo, *Adv. Funct. Mater.* **2018**, *28*, 1707520.

[9] J. Zhang, H. Huang, J. Bae, S. H. Chung, W. K. Zhang, A. Manthiram, G. H. Yu, *Small Methods* **2018**, *2*, 1700279.

[10] a) I. Bauer, S. Thieme, J. Bruckner, H. Althues, S. Kaskel, *J. Power Sources* **2014**, *251*, 417–422; b) T. Z. Zhuang, J. Q. Huang, H. J. Peng, L. Y. He, X. B. Cheng, C. M. Chen, Q. Zhang, *Small* **2016**, *12*, 381–389.

[11] J. Q. Huang, T. Z. Zhuang, Q. Zhang, H. J. Peng, C. M. Chen, F. Wei, *ACS Nano* **2015**, *9*, 3002–3011.

[12] a) S. Y. Bai, X. Z. Liu, K. Zhu, S. C. Wu, H. S. Zhou, *Nat. Energy* **2016**, *1*, 16094; b) H. Q. Jiang, X. C. Liu, Y. S. Wu, Y. F. Shu, X. Gong, F. S. Ke, H. X. Deng, *Angew. Chem. Int. Ed.* **2018**, *57*, 3916–3921; *Angew. Chem.* **2018**, *130*, 3980–3985.

[13] G. R. Li, F. Lu, X. Y. Dou, X. Wang, D. Luo, H. Sun, A. P. Yu, Z. W. Chen, *J. Am. Chem. Soc.* **2020**, *142*, 3583–3592.

[14] X. Liang, Y. Rangom, C. Y. Kwok, Q. Pang, L. F. Nazar, *Adv. Mater.* **2017**, *29*, 1603040.

[15] a) Z. H. Sun, J. Q. Zhang, L. C. Yin, G. J. Hu, R. P. Fang, H. M. Cheng, F. Li, *Nat. Commun.* **2017**, *8*, 14627; b) T. H. Zhou, W. Lv, J. Li, G. M. Zhou, Y. Zhao, S. X. Fan, B. L. Liu, B. H. Li, F. Y. Kang, Q. H. Yang, *Energy Environ. Sci.* **2017**, *10*, 1694–1703.

[16] a) Z. A. Ghazi, X. He, A. M. Khattak, N. A. Khan, B. Liang, A. Iqbal, J. X. Wang, H. S. Sin, L. S. Li, Z. Y. Tang, *Adv. Mater.* **2017**, *29*, 1606817; b) N. K. Thangavel, D. Gopalakrishnan, L. M. R. Arava, *J. Phys. Chem. C* **2017**, *121*, 12718–12725.

[17] a) Y. Li, J. Wu, B. Zhang, W. Wang, G. Zhang, Z. W. Seh, N. Zhang, J. Sun, L. Huang, J. Jiang, J. Zhou, Y. Sun, *Energy Storage Mater.* **2020**, *30*, 250–259; b) Y. Li, C. Wang, W. Wang, A. Y. S. Eng, M. Wan, L. Fu, E. Mao, G. Li, J. Tang, Z. W. Seh, Y. Sun, *ACS Nano* **2020**, *14*, 1148–1157; c) J. Xie, B.-Q. Li, H.-J. Peng, Y.-W. Song, M. Zhao, X. Chen, Q. Zhang, J.-Q. Huang, *Adv. Mater.* **2019**, *31*, 1903813.

[18] J. Zhou, T. Qian, N. Xu, M. Wang, X. Ni, X. Liu, X. Shen, C. Yan, *Adv. Mater.* **2017**, *29*, 1701294.

[19] S. Fan, S. Z. Huang, M. E. Pam, S. Chen, Q. Y. Wu, J. P. Hu, Y. Wang, L. K. Ang, C. C. Yan, Y. M. Shi, H. Y. Yang, *Small* **2019**, *15*, 1906132.

[20] a) P. D. Frischmann, L. C. H. Gerber, S. E. Doris, E. Y. Tsai, F. Y. Fan, X. H. Qu, A. Jain, K. A. Persson, Y. M. Chiang, B. A. Helms, *Chem. Mater.* **2015**, *27*, 6765–6770; b) H. Ye, J. Y. Lee, *Small Methods* **2020**, *4*, 1900864.

[21] a) J. B. Park, S. H. Lee, H. G. Jung, D. Aurbach, Y. K. Sun, *Adv. Mater.* **2018**, *30*, 1704162; b) H. Zhang, G. G. Eshetu, X. Judez, C. M. Li, L. M. Rodriguez-Martinez, M. Armand, *Angew. Chem. Int. Ed.* **2018**, *57*, 15002–15027; *Angew. Chem.* **2018**, *130*, 15220–15246.

[22] a) S. Chen, Y. Gao, Z. Yu, M. L. Gordin, J. Song, D. Wang, *Nano Energy* **2017**, *31*, 418–423; b) W. Guo, A. Bhargav, J. D. Akkerson, Y. Cui, Y. Ma, Y. Fu, *Chem. Commun.* **2018**, *54*, 8873–8876; c) M. Wu, A. Bhargav, Y. Cui, A. Siegel, M. Agarwal, Y. Ma, Y. Fu, *ACS Energy Lett.* **2016**, *1*, 1221–1226.

[23] S. Y. Wei, S. M. Xu, A. Agrawral, S. Choudhury, Y. Y. Lu, Z. Y. Tu, L. Ma, L. A. Archer, *Nat. Commun.* **2016**, *7*, 11722.

[24] S. R. Chen, D. W. Wang, Y. M. Zhao, D. H. Wang, *Small Methods* **2018**, *2*, 1800038.

[25] G. Zhang, Z. W. Zhang, H. J. Peng, J. Q. Huang, Q. Zhang, *Small Methods* **2017**, *1*, 1700134.

[26] Q. Wang, J. M. Zheng, E. Walter, H. L. Pan, D. P. Lv, P. J. Zuo, H. H. Chen, Z. D. Deng, B. Y. Liaw, X. Q. Yu, X. Q. Yang, J. G. Zhang, J. Liu, J. Xiao, *J. Electrochem. Soc.* **2015**, *162*, A474–A478.

[27] a) J. Guo, M. G. Zhang, X. Y. Yan, S. S. Yao, X. Y. Cao, J. S. Liu, *J. Nanopart. Res.* **2019**, *21*, 70; b) F. Wu, J. Z. Chen, L. Li, T. Zhao, Z. Liu, R. J. Chen, *ChemSusChem* **2013**, *6*, 1438–1444.

[28] a) H. Chu, H. Noh, Y. J. Kim, S. Yuk, J. H. Lee, J. Lee, H. Kwack, Y. Kim, D. K. Yang, H. T. Kim, *Nat. Commun.* **2019**, *10*, 188; b) A. Gupta, A. Bhargav, A. Manthiram, *Adv. Energy Mater.* **2019**, *9*, 1803096; c) Q. L. Zou, Y. C. Lu, *J. Phys. Chem. Lett.* **2016**, *7*, 1518–1525; d) K. H. Wujcik, T. A. Pascal, C. D. Pemmaraju, D. Devaux, W. C. Stolte, N. P. Balsara, D. Prendergast, *Adv. Energy Mater.* **2015**, *5*, 1500285; e) G. Zhang, H. J. Peng, C. Z. Zhao, X. Chen, L. D. Zhao, P. Li, J. Q. Huang, Q. Zhang, *Angew. Chem. Int. Ed.* **2018**, *57*, 16732–16736; *Angew. Chem.* **2018**, *130*, 16974–16978.

[29] a) N. I. Kim, C. B. Lee, J. M. Seo, W. J. Lee, Y. B. Roh, *J. Power Sources* **2004**, *132*, 209–212; b) Y. L. Li, J. J. Wang, X. F. Li, D. S. Geng, M. N. Banis, Y. J. Tang, D. N. Wang, R. Y. Li, T. K. Sham, X. L. Sun, *J. Mater. Chem.* **2012**, *22*, 20170–20174; c) C. Tan, T. M. M. Heenan, R. F. Ziesche, S. R. Daemi, J. Hack, M. Maier, S. Marathe, C. Rau, D. J. L. Brett, P. R. Shearing, *ACS Appl. Energy Mater.* **2018**, *1*, 5090–5100.

[30] a) J. Liang, L. C. Yin, X. N. Tang, H. C. Yang, W. S. Yan, L. Song, H. M. Cheng, F. Li, *ACS Appl. Mater. Interfaces* **2016**, *8*, 25193–25201; b) Y. Q. Tao, Y. J. Wei, Y. Liu, J. T. Wang, W. M. Qiao, L. C. Ling, D. H. Long, *Energy Environ. Sci.* **2016**, *9*, 3230–3239.

Manuskript erhalten: 26. Juni 2020
Akzeptierte Fassung online: 21. August 2020
Endgültige Fassung online: 25. September 2020

